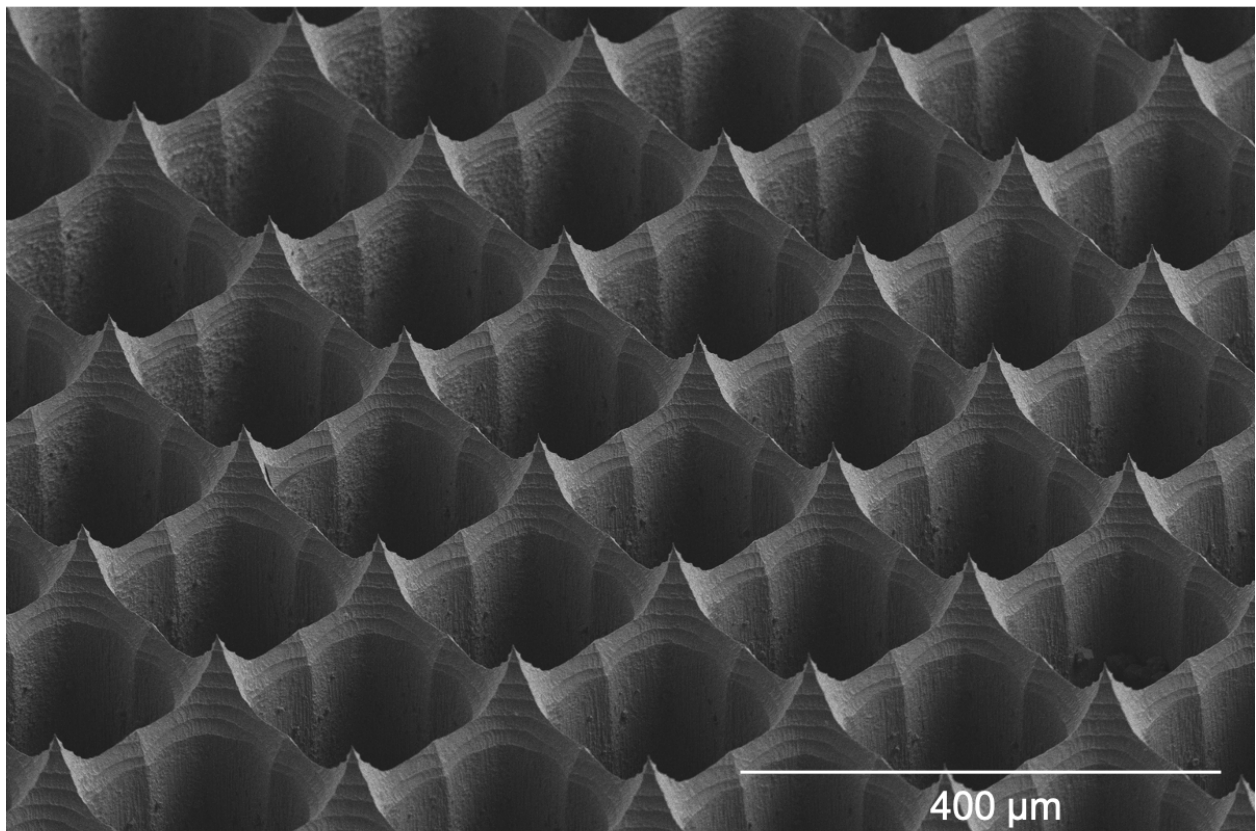# Fabrication of an Etched Silicon Platform with Applications in Uniform Dissection of Biological Samples

ENGR 241 Winter Quarter Final Report
Nicolas Castaño, Seth Cordts, Saisneha Koppaka
SNF Lab Mentors: Usha Raghuram, Antonio Ricco, Mark Zdeblick

Acknowledgements

Introduction

Motivation

Background: In 2018 approximately 1.7 million people in the United States were diagnosed with cancer. Cancer is an extremely heterogeneous disease, and one of the key challenges lies in predicting the efficacy of drugs on individual patients. While there are diagnostic methods based on sequencing the cancer genome, these methods are limited because they cannot account for the specific tumor microenvironment (TME). The TME modulates several components of tumorigenesis including initiation, progression, and metastasis. Recent studies show that TME is an increasingly crucial player in modulating the response of cancer cells to chemotherapy [1]. While it would be most useful to test drug assays using tumor biopsy samples directly, samples are often limited in amount and size, demanding the need for model-based methods. Within *ex vivo* models of the TME, patient-derived organoids (PDOs), which are organ-like tumor tissues, have been shown to maintain both the organization and physiological structure of the source tumor. PDOs are thus promising platforms for advancing personalized cancer therapeutics.

Challenges. The use of mechanical dissection of tissue into smaller fragments, instead of enzymatic digestion, is critical to the success of PDO preparation to preserve the TME. However, the current methods of mechanical dissection are inadequate: they are either slow or imprecise, and they are not amenable to multiplexed drug screening. Specifically, PDOs are typically generated by manual mechanical dissection (e.g. mincing) of tissues [2]. Much care is needed in mincing tumor-cell rich nodules for the best chance of success in their isolation. Due to the variability of manual mincing, a board range of fragment sizes (ranging from tens of microns to centimeters) are generated. It is unclear how many of the fragments can recapitulate the actual TME. While methods such as laser-based microdissection of tissue allow more precise control of fragment size, they remain expensive and time-intensive, and still require downstream manual handling of dissected samples for subsequent analysis or drug screening.

Thus, there is a **critical unmet need** for a reproducible, high-throughput method to generate uniform-sized tissue fragments for PDOs that can preserve the TME while remaining compatible with subsequent multiplexed drug screening. The overall **objective** of this work is to address this need by developing a microfabricated device, referred to as the "µTissue Dicer," to dissect tissues

into uniform-sized sub-millimeter fragments in a reproducible, high-throughput manner, and to interface the μDicer with microfluidics for subsequent multiplex drug screening of organoids.

Our method is expected to accelerate the tissue dissection process for PDOs and subsequent drug screening assays. Achieving this project goal will be **<u>significant</u>,** as it will 1) standardize the preparation for PDOs, which is critical for its wider clinical adoption, 2) accelerate the tissue dissection, analysis, and drug screening process by allowing more PDOs to be tested in a multiplexed and streamlined fashion, 3) generate fundamental insight into how initial fragment size affects cell type diversity, the tumor microenvironment, and drug response.

Exploratory Aim in Regeneration

While the primary motivation of our device is uniform tissue dissection for the purpose of PDO preparation, we have also envisioned the potential of our device in studying regeneration. In particular, the planarian worm is a good case study: the worm is able to regenerate the whole organism from individual fragments. While this is an exploratory aim at the moment, we envision that our device can enable both fundamental and application-based studies in regenerative medicine. During this project, we briefly tested dicing planarian worms using our device. Ongoing work in our group will refine and test the μDicer for regeneration.

Project Concept and Vision

Our aim is to optimize the silicon-etched microdevice for generating both fresh and fixed tissue of various origins (ranging from soft lung tissue to stiffer breast tissue) into uniform sections of 50 μm to 200 μm in their longest dimension. The geometries of the blade will be optimized to ensure minimum loss of intrinsic cells in tumor biopsies having different stiffnesses. The tissue section will be driven through the blades using a pressure differential (See Figure 1 for a schematic diagram of the device). Alternatively, centrifugal force may be used. Our etched silicon device will then be interfaced with optically clear microwells for downstream drug screening that will be fabricated with 3D printing or soft lithography. We will evaluate the success of our device based on the uniformity of the resultant fragments and their ability to recapitulate the tumor architecture and fibroblast stroma.
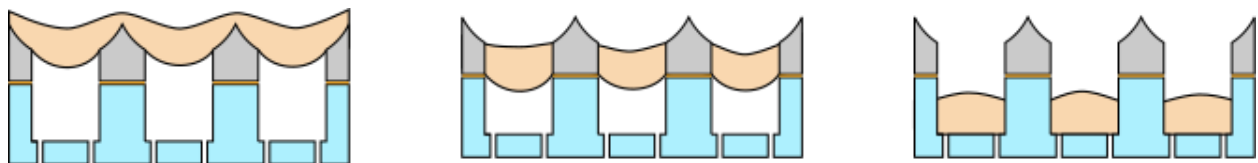
Our downstream experiments are to determine the relationship between tissue fragment size, PDO viability, immune diversity in PDOs, and the corresponding drug response. We envision that our μTissue Dicer will enable high throughput, high spatial resolution, and unbiased preparation of

tissue fragments and facilitate multiplexed drug screening in PDOs. Our method is expected to be useful not only for PDOs but also for other applications that require organotypic cultures.

This leads us to four primary objectives during our realization of this project:
Objective 1: Optimize etch recipe for fabricating arrays of angled blades by tuning C_4F_8:SF_6 gas ratio, etch time, and bias voltage to produce etch profiles that are not quite isotropic, yet also not crystal plane dependant (termed pseudo-isotropic).
Objective 2: Test etched devices against tissue phantom with compression test to validate cutting ability.
Objective 3: Etch through-holes in wafer to allow for tissue to be extruded through device and strengthen cutting surface by passivation with a robust metal (i.e. platinum).
Objective 4: Integrate bladed array with an extruding force to draw tissue through the device into collection microwells for subsequent biological analysis.
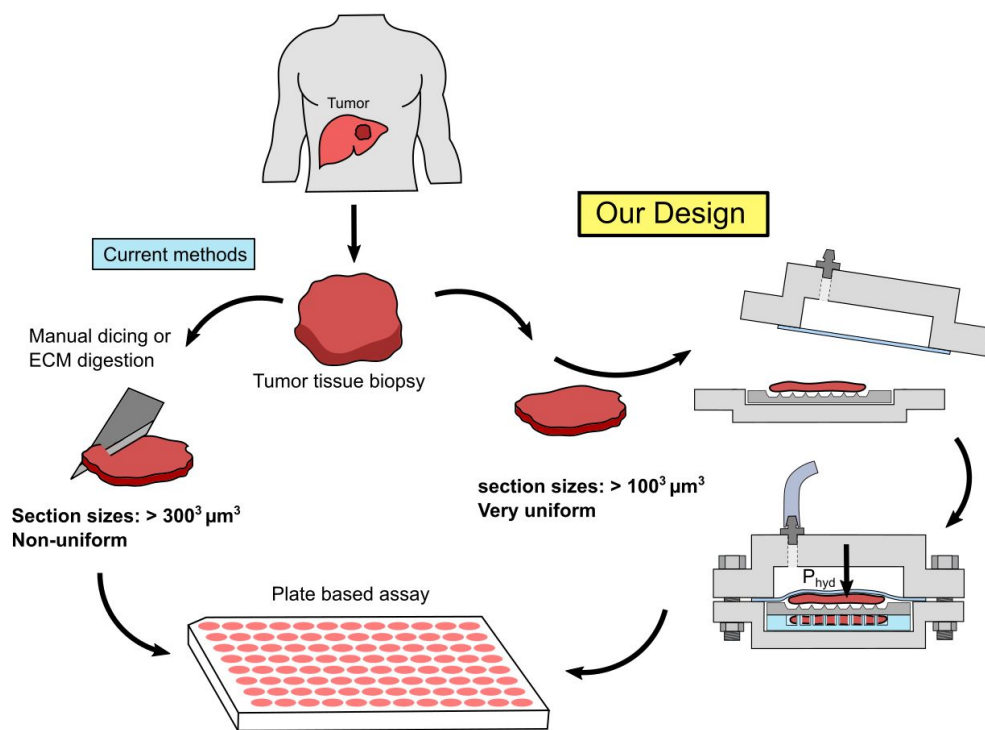
Figure 1: *Conceptual sketch comparing our device functionality and comparing to current methods of manual mincing tumor tissue.*

Benefits to the SNF Community

Fall Quarter: While working towards our project goals of pseudo-isotropic etching of silicon to form "blades" along with some supplementary objectives, we contributed the following characterizations to the SNF community:
- Characterize the degree of undercut and corresponding blade geometry of an oxide-masked etch of silicon using SF_6 and C_4F_8 gases in the PT-DSE
- Characterize oxide etch rate in PT-DSE varying SF_6 and C_4F_8 gasses

- Investigate non-conventional uses of the PT-DSE for pseudo-isotropic etch profiles
- Investigate and report on the potential of using multi-stage PT-DSE recipes for single mask pseudo-isotropic etching and Bosch process etching

Winter Quarter: While working towards our project goals of through-etching a silicon wafer, characterizing cutting efficiency, and interfacing with microwells, we continued to benefit the SNF community by producing SOPs for:

- Through-wafer etching by bulk etching with PT-DSE: addressing problems of bottom grassing, mask buckling, and maintain mask shape at the bottom of through-wafer etch
- Micromilling microwells and/or using soft-lithography to integrate with etched silicon blades. Best methods for interfacing the two aspects of such a system
- Potential methods for extending the life of etched structures by passivating silicon with a metal or fabricating duplicates with cheaper materials
- Python script for determining the etch profile

We have developed a standard operating procedure on how to utilize and develop recipes on the PlasmaTherm Deep Silicon Etcher (PT-DSE) for the purpose of (1) achieving a specific tapered angle etch and (2) through-etching a 500 μm wafer is included with this report. Additionally, we have developed a python script for predicting the etch profile of a structure. The script will be available for the general SNF community to download and adapt as necessary. Finally, the SNF users will also be provided an SOP on interfacing etched silicon with microwells.

Fabrication and Experimental Methods
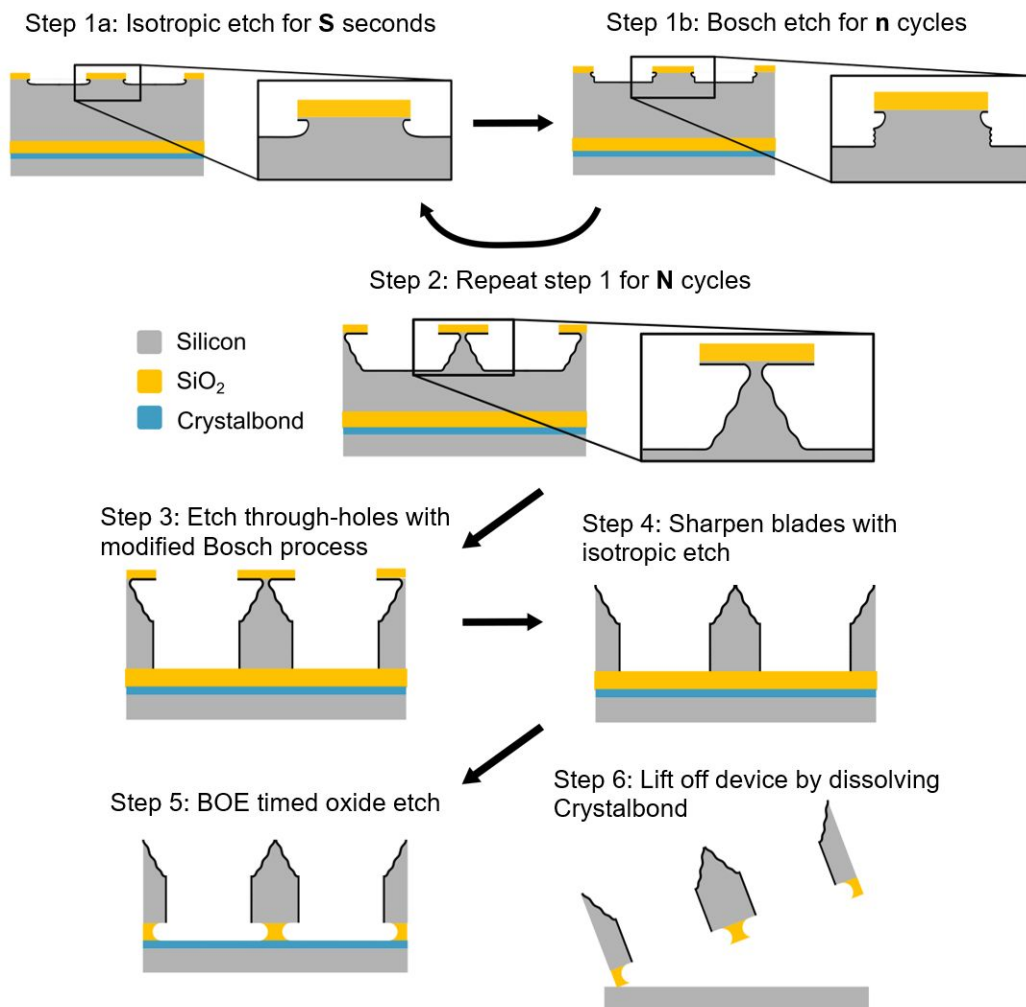
Tools Utilized in Process

Specific run and recipe details of pertinent processes are outlined in the Appendix. The following tools were used in the fabrication:

- PlasmaTherm Shuttlelock SLR-730-PECVD for capacitively coupled plasma deposition (CCP-DEP) of oxide on silicon.
- YES Prime Oven for dehydrating wafers at 150℃ and priming with HMDS (Hexamethyldisilazane) allowing better coverage and adhesion between oxides and resists.
- SVG Resist Coat for resist coating
- SVG Resist Develop for resist development
- Heidelberg 1 for patterning photoresist
- Technics Plasma Asher
- Matrix Plasma Asher to clean wafer between etching cycles
- Samco Ozone Cleaner to clean wafer between etching cycles
- 6:1 BOE (34% Ammonium fluoride (NH_4F), Hydrofluoric acid 7%, 59% water) oxide etch
- Piranha (70% - 90% sulfuric acid (H_2SO_4), hydrogen peroxide(H_2O_2)) photoresist strip
- PlasmaTherm Deep Silicon Etch of silicon using an oxide hard mask
- Apreo Scanning Electron Microscope Nanospec2, and Keyence Digital Microscope VHX-6000 for characterizing mask thickness and resultant etches
- Lesker Sputter Deposition Tool for Pt thin film to increase blade strength

● Oxford PlasmaPro 80 - Reactive Ion etcher was important for initial prototyping.

Overall Process Flow

Our goal was to fabricate blades that are at least ~20° sharp, which is approximately the radial angle of a surgeon's scalpel.Our fabrication process primarily uses the PTDSE to etch the tapered structure forming blades, and the through-holes. The tapered etch process was inspired by [3].We experimented with various etch recipes and gas compositions for our fabrication process and converged to our final process which consists of Isotropic etching and Bosch process etching. For our blade etching experiments, we modify the Isotropic etch time, **S**, the number of Bosch cycles per loop, **n**, and the number of loops, **N** (Steps 1-2). For the through-hole experiments, we experimented with the morphing feature in the PT-DSE software to increase the RF bias voltage as we etched deeper into the silicon (Step 3). Other parameters such as gas ratios, mask material were also modified during the course of the project and these results and how we settled on the final choices will be included in the appendix.

Step 1a: Isotropic etch for **S** seconds

Step 1b: Bosch etch for **n** cycles

Step 2: Repeat step 1 for **N** cycles

Silicon
SiO$_2$
Crystalbond

Step 3: Etch through-holes with modified Bosch process

Step 4: Sharpen blades with isotropic etch

Step 5: BOE timed oxide etch

Step 6: Lift off device by dissolving Crystalbond

Silicon Etching Parameters

A significant portion of the fall quarter dealt with optimizing and testing various etch conditions using the PlasmaTherm Dry Silicon Etcher (PT-DSE), which is an inductively-coupled-plasma etch system that's traditionally configured for silicon etches using the Bosch process.

The following is a table containing a column of parameters that can be changed on the PT-DSE to vary the etch profile. The second column contains the effect of increasing the parameter. In the appendix, our SOP includes a section on how to debug errors that may arise on the PT-DSE.

Table 1: *Etch experimental parameters*

| Parameters	Effect
Bias RF Voltage Setpoint (V)	Vertical etch rate; Mask selectivity
$C_4F_8 : SF_6$ Gas Ratio (or $SF_6 : O_2$, which was not explored in this project) (sccm:sccm)	Degree of undercut; Horizontal to vertical etch rate ratio
ICP Match Tune Position Setpoint (W)	ICP RF Reflected Power
Blade angle: Number of iterations (N) of Bosch cycles (n) + isotropic etch time (S)	Increasing n for a fixed S increases the blade sharpness
Temperature electrode setpoint (°C)	*Difficulty in attempting this characterization (e.g. It can take over an hour for the electrode temperature to stabilize to 35°C)*

Updated Mask Design

We modified the mask designs to experiment with serrated blades vs non-serrated blades in the µDicer. As seen in Figure 3, The Mask opening geometry controls where or not a serration is formed for two devices with the same etching recipe.
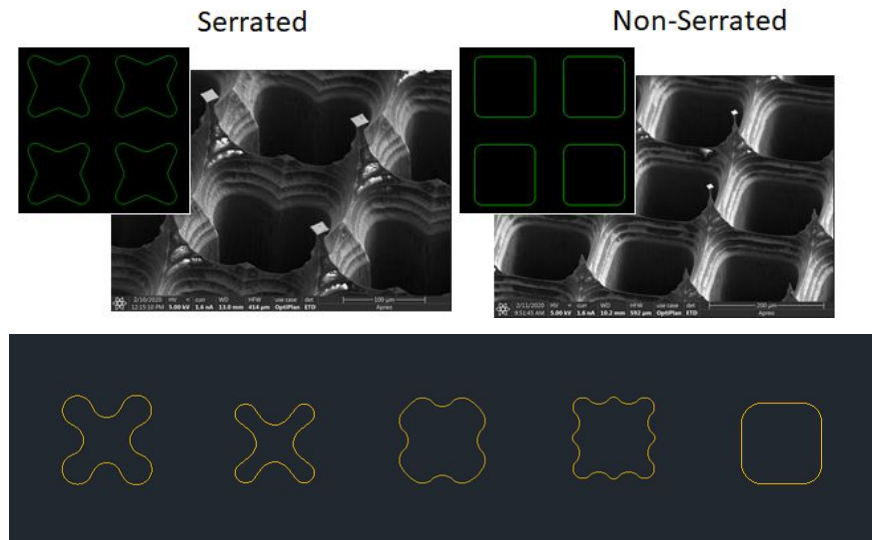
Figure 3: *How mask design can lead to serrated blades. An example of a* µDicer *device with serrated blades is on the upper left and non-serrated blades is on the . Various other mask designs were tested. Some of these are referenced in the Table 2 and defined in the Appendix.*

Method for Measuring Blade Angle Using SEM Images

To determine the angle of the resultant tapered etches and thus, the blades, we used our SEM images. However to get an accurate reading we had to account for the SEM Stage tilt. The angle is measured by taking the arctan of the X measurement divided by the Y measurements as seen in Figure 4. However, the Y dimension must be corrected due to the SEM stage tilt angle.


$$\theta_{bl} = \tan^{-1}(x \ * \ \frac{\cos(\theta_{tilt})}{y})$$
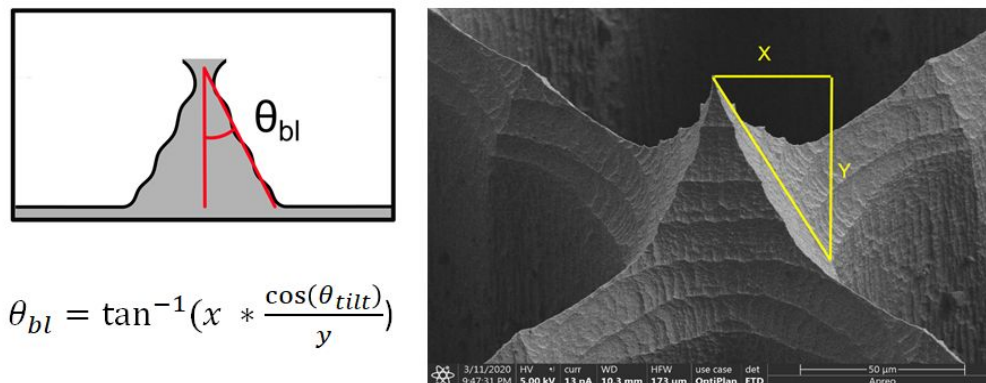
Figure 4: *The blade half-angle is calculated using the equation in the bottom left and takes into account correction for the SEM stage tilt angle.*

Experimental Protocol for Evaluating Tissue Cutting Effectiveness

There are some nuances to the strength of biological tissue that stem from their viscoelastic behavior. As viscoelastic materials, biological tissues exhibit strain rate rate dependance, whereby lower loading rates result in the viscoelastic materials behaving more viscous and compliant and higher loading rates lead to a more elastic and rigid response. These are important properties of biological material to keep in mind when designing experiments to test the effectiveness of our blade array and the tissue analogs we are using. Herein lie some crucial considerations to take when designing a method to extrude tissue through our final blade array.

Similar to our tissue cutting experiment from the fall quarter, we tested both the cutting ability and mechanical strength of our etched blade array. To test cutting ability, we used porcine articular cartilage harvested by the Soft Tissue Biomechanics Lab as an analog for tumor organoids. Cartilage has an elastic modulus (effectively stiffness) ranging from 0.4 to 27 MPa depending on loading conditions and time scale [4] while tumor organoids exhibit stiffness on the order of 100 Pa to 5 kPa [5]. Thus, in terms of evaluating the blades ability to cut through a tough biological material, cartilage as an analog provides a conservative predictor, however with the properties of viscoelasticity in mind a softer, more compliant tissue could prove to be more challenging to cleanly section. We also tested a sample of mouse melanoma tumor tissue, and noted that it was much softer than cartilage tissue.
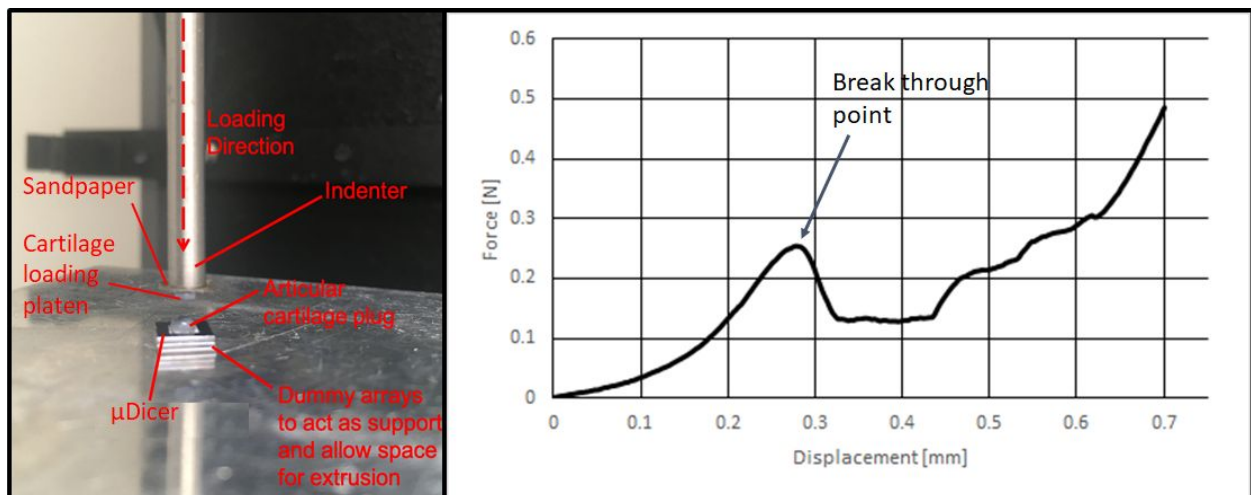
Figure 5: Experimental setup on Instron for to produce force-displacement curve that shows the point at which cartilage broke through and began extruding through the µDicer. Sandpaper was used to prevent sliding of the cartilage loading platen on the tip of the indenter.

We demonstrated the cutting ability with cartilage. In particular this test demonstrates the strength of the µDicer against extrusion of tough tissue. Figure 6 shows some sections of cut cartilage. It shows the uniformity of the section size and well defined edges formed by the µDicer. For these cut tests, we selected µDicers based on (1) the size of the through-hole, and (2) the presence of a

pointed tip or a small plateau at the tip. This is to say that tissue cutting effectiveness was most dictated by the presence of clean through-holes and the ability to initiate a cut at a tip.
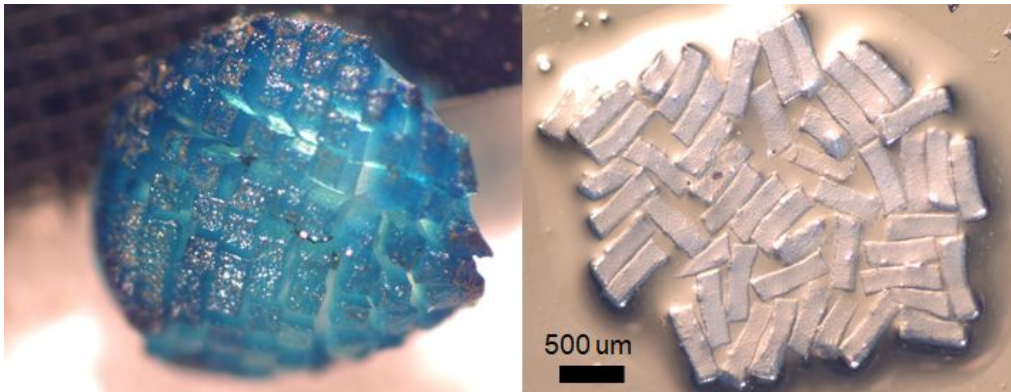
Figure 6: Partially cut cartilage dyed blue to highlight well defined edges (left). Fully extruded cartilage sections of uniform size (right).

System Integration

To use our µDicer effectively we need to integrate it with a system for loading and extruding tissue through it. To do so, we first explore a vacuum driven system to pull tissue through the device but we were not able to generate enough force to pull the tissue through. We determined that a pressure driven system might work best using hydraulic pressure. The device consists of a PMMA chamber to hold the µDicer, microwells, and tissue sample and a mating PMMA chamber that has a silicone membrane separating the tissue from the hydraulics. The device functions using hydraulic pressure to deform the silicon membrane and press the tissue through the µDicer and into the microwells. The PMMA chambers were laser cut and machined in the SNF using the laser cutter and Minitech GX Micromill.
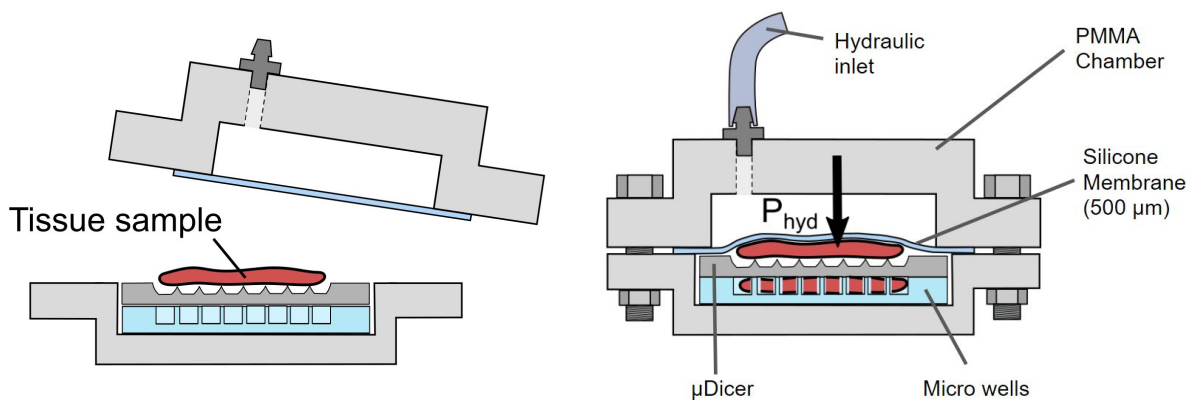
Figure 7: schematic of the pressure chamber for dicing tissue with the µDicer. The microwells, µDicer, and tissue sample are placed into the bottom half of the device (Left). Then, the top half is secured to the bottom half with bolts. The hydraulic pressure extrudes the tissue through the µDicer.

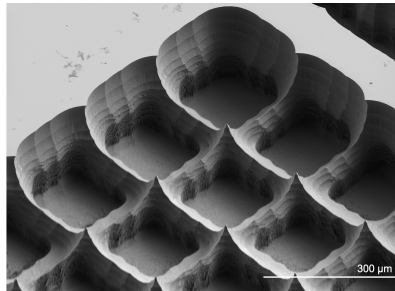# Results and Discussion

Etching Characterization

Table 2 includes a compilation of the blade etch and through etch parameters that we studied over the course of the winter quarter. The rows are listed in chronological order of when we attempted the etch. In the later iteration of the etches (i.e. in the later rows) the etched blades are much sharper-- they meet our goal criterion to be at least as sharp as a surgeon's scalpel!

Our characterization shows that for a given blade isotropic etch time (S), increasing the number of Bosch loops (n) decreases the blade angle. For instance, increasing the number of Bosch loops from 10 loops to 15 loops for a 100 s isotropic etch decreased the blade angle from 25.8° to 20.1°. On the other hand, increasing the number of cycles N increases the vertical height of our blades, reducing the number of cycles to through-etch the wafer.
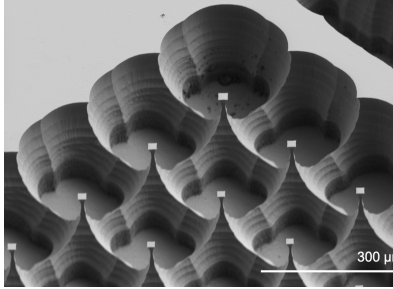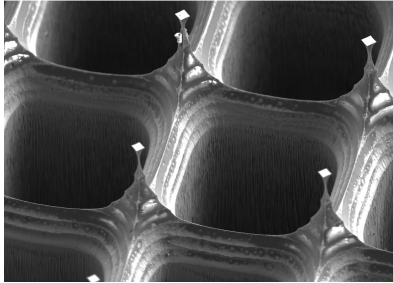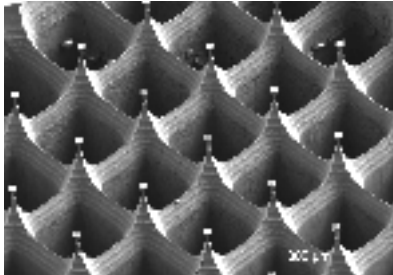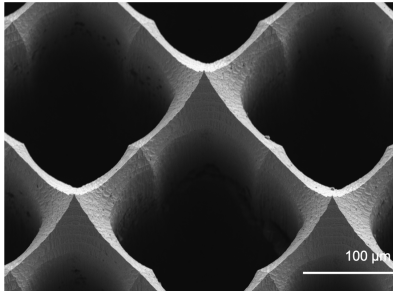
Note 1: A few of the SEMs below contain a small plateau at the top of the blades. In these cases, we did not etch long enough for the etch fronts to fully meet.
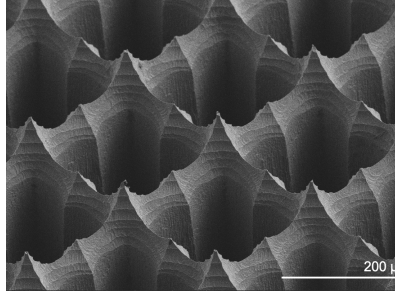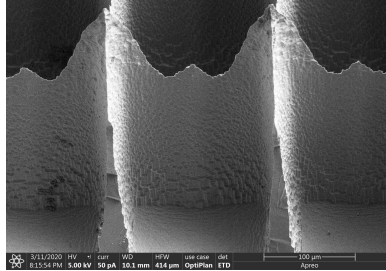Note 2: All angle measurements account for the tilt of the SEM stage.

__Table 2:__ Etch experimental conditions and results

Blade etch parameters			Through etch parameter	Results	
Number of Cycles (N)	# of Bosch Loops (n)	Isotropic etch time (S)	Cycles to Through-Etch (+ iso etch time*(s))	Blade half angle (θ_{bl})	SEM Image (Lookup ID given, see Appendix)
14	10	100	350	24.6°	(R6C3)

7	10	100	N/A	25.2°	 (R7C3)
7	10	100	435 Note: Did not end up etching through the wafer with 435 cycles.	24.3°	 (R2C3)
7	13	100	550 (+ 50 s)	23.4°	 (R3C4)
7	10	100	550 cycles**	25.8°	 (R5C3)

7	15	100	550 cycles**	20.1°	 (R4C3)
5	13	100	550 cycles** 50 cycles at 400V	6°	 (R5C1)

Isotropic etch time (s) has 0:300 C_4F_8 : SF_6. Note that the Isotropic etch time (S) to form the blades has 50:300 C_4F_8 : SF_6. We decided that the etch to clear bottom grassing should have no polymer passivation, while the etch to form the blades would benefit from some passivation.

**Morphed Etch A Bias Voltage. Please refer to our SOP and our NanoNuggest section on 'Through- Wafer Dry Etching' information on morphing features.*

*** This markedly sharp angle was in a region of mask collapse. It is an excellent target sharpness that came about through some local conditions that remain somewhat of a mystery. It should be noted that this array was located at the periphery of the wafer (one possible reason why the etch did not break through all the way).*

We found that the task of taking angle measurements was highly variable (only the average of several measurements was reported above, with standard deviation as large as ± 4.8° in some cases). The resulting etch profile of a given blade array was a function of position on wafer, spacing between features, and local integrity of mask. The last point was especially important as some regions of collapsed masks resulted in rough surface finishes. While not ideal, we did find that blade arrays with rough finishes were still structurally sound and could with standstand high loads during testing without breaking. Figure 8 shows macroscopic and zoomed in images of one array that was used to cut agar.
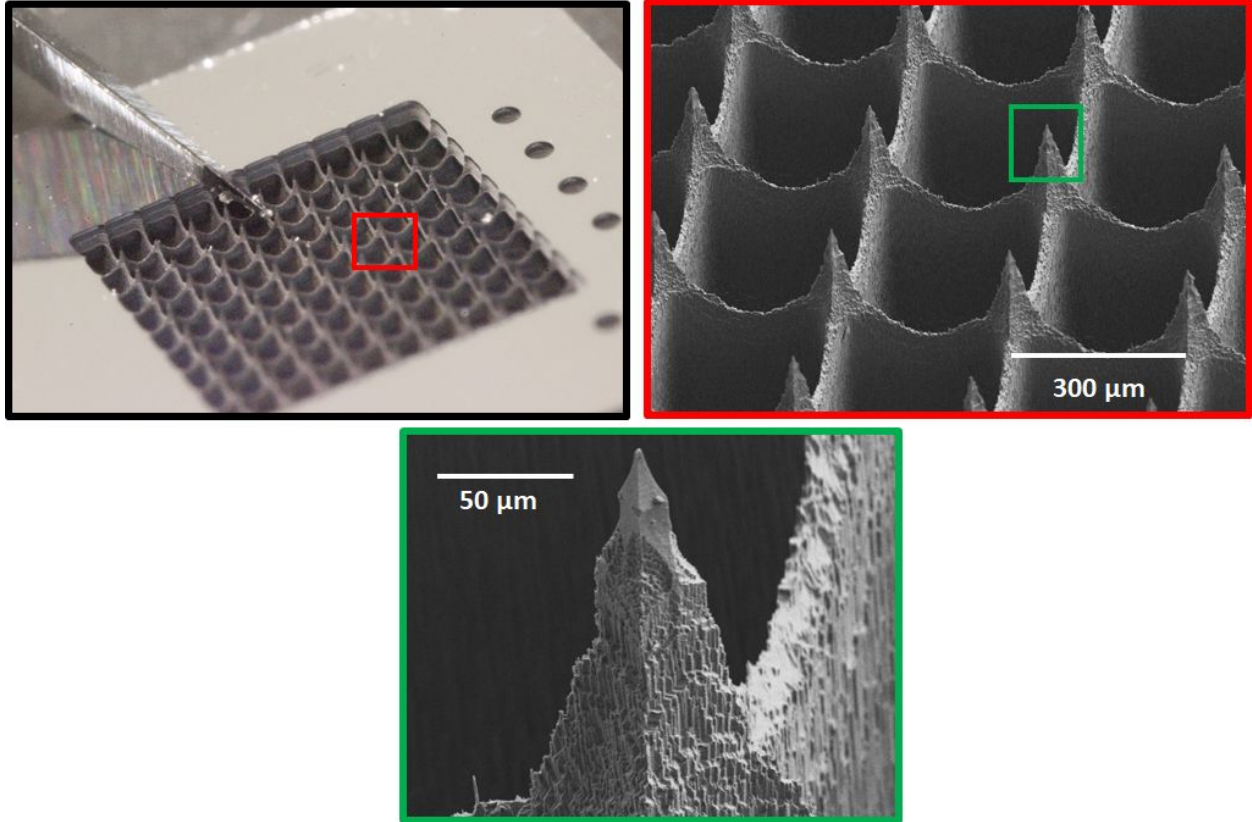
Figure 8: *Zoomed in views of a bladed array and an individual tip. The upper left image shows a surgeon's scalpel for sharpness reference.*

We hypothesize that the rough finish in regions of mask collapse are a result of the Bosch process acting on an inclined face (not perfectly horizontal or vertical). In Figure 8, it should be noted that the tip sustained an island of mask which is why the surface is smooth near the tip. Where the mask could not cover was exposed to Bosch cycles. Inclined regions finished with a rough surface while vertical regions were smoother.

System Integration

We were unable to complete all of the testing with the pressure chamber before the end of the course, but we were able to dice 2% agarose gels (tissue phantom) using the μDicer with large through-holes (~600μm). For the device with smaller through-holes (~200μm) there was too much resistance and the agar was soft enough to deform around the device instead of extruding through. This is partly due to the through-holes having a slight necking effect in the bottom, which adds a lot of resistance to the tissue passing through. For the small μDicer, we were able to dice agar by manually pressing the hydrogel through the device [Figure 9]. The results for dicing agar with the large μDicer are shown in Figure 10.
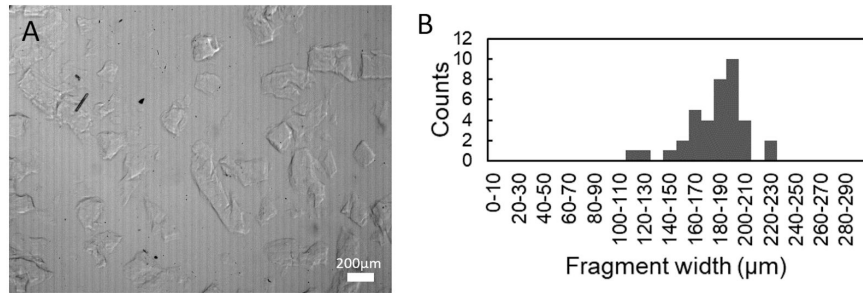
Figure 9: *A) Resultant fragments after manually extruding an agar sample through the μDicer with smaller openings. B) Size distribution of fragment widths from A.*
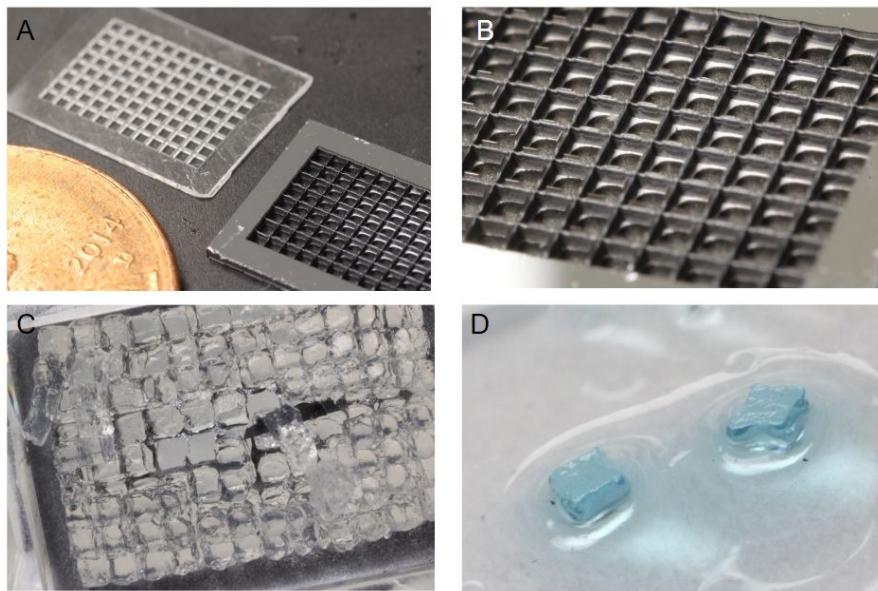

Figure 10: *A) a large μDicer next to a PMMA micromilled microwell and a penny . B) A close up image of the same device from A. C) An image of 2% agar being extruded through the large μDicer using the pressure chamber. D) Two resultant pieces from C dyed blue for contrast and imaging.*

Modeling Initiative

As part of our contribution to the SNF we aimed to develop a Python script for modeling the evolution of an etch recipe in the PT-DSE up to the final form of the etched product. This is meant to provide an open source tool to the SNF community that can aid in designing novel structures.

During the Winter quarter, this model underwent two major version changes. The first was a rudimentary solver that created layers of etching which were only lowered in elevation (to model Bosch process), but not evolved in a physically meaningful way after initializing. The second, and most current (still under development as of now), version seeks to evolve a 3D surface using normal vectors and an approximated displacement field. In contrast with version 0, the version 1 model evolves all parts of the etch surface each time step is consistent with the step (i.e., Bosch

steps only drop the surface contained within the x, y boundaries of the mask). Unit normal vectors of a given mesh point are multiplied by a displacement field that is approximated with a quadratic function that encompasses user prescribed vertical and horizontal etch rates. The current version also uses vtk rendering capabilities to produce interactive models that can be saved.
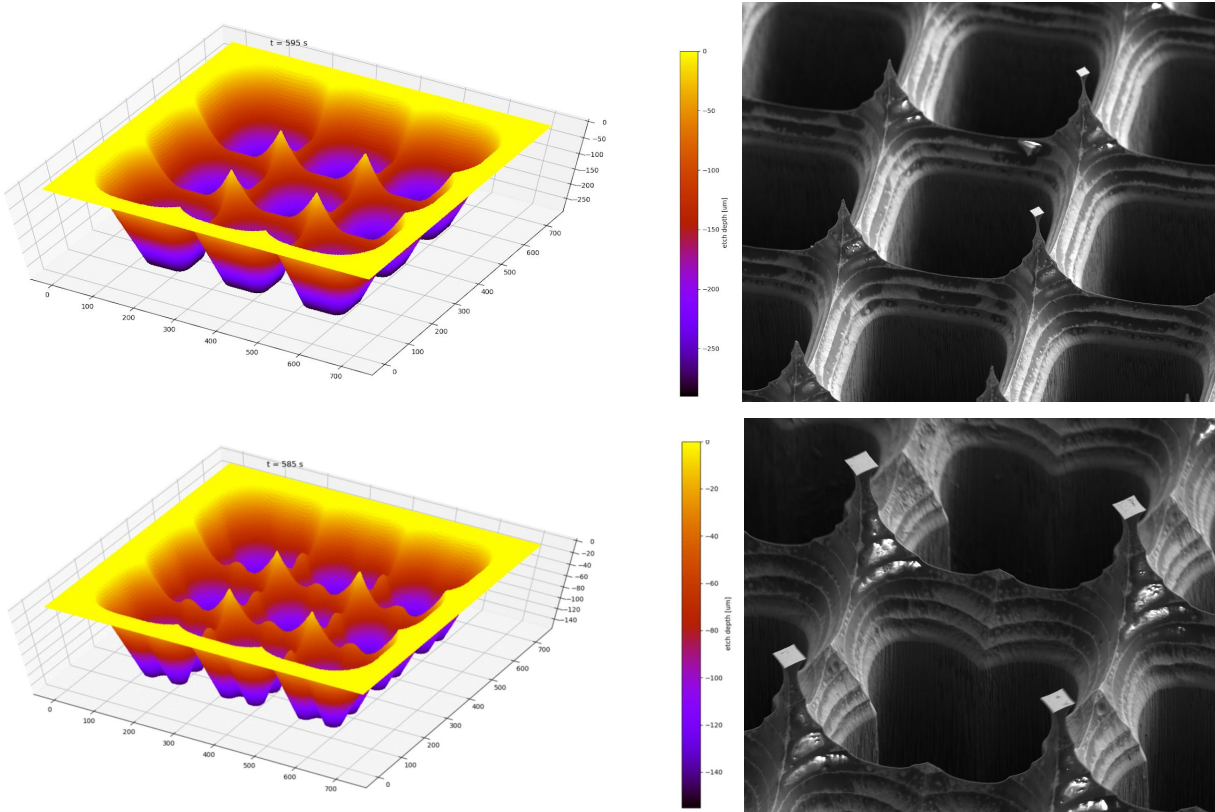
Figure 11: *Screenshots from the version 0 model for two different etch mask designs (Left) and the comparable SEM images for the etched devices.*

The code is hosted on Github at: https://github.com/cococastano/PythonDryEtchModel. It is our hope that this code is iterated upon apart from the continued development we aim to pursue.

Future Work

Our work from these last two quarters has helped us prototype and develop the key components of the μDicer. We found no shortage of knobs to turn in tweaking specific aspects of our design, but we have settled on a process flow and PT-DSE recipe that have produced promising results. In the future, we will fine tune the etch parameters and mask design, improve etch reproducibility (i.e., expect the same result from the same process flow with each new etch), further characterized our etching results (i.e., tip angle), and continue with system integration and testing of the device. We intend to share any additional documentation that we produce with the SNF community as this project is an exciting jumping off point for a promising branch of continued research we will do in our lab.

Appendix

Budget

The chart below represents the breakdown of our winter quarter budget. The majority of our investment this quarter went into preparing the wafers (oxide deposition, patterning, and wet bench) and then etching and imaging our result (plasma etching, imaging on Apreo SEM and Keyence Microscope). Unlike the fall quarter, training only consumed about 3.7% of our budget and the material costs were primarily for buying new wafers and crystalbond.
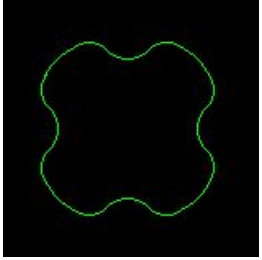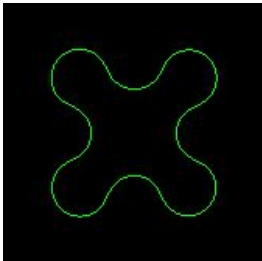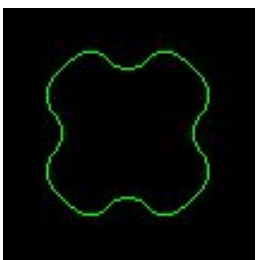

Winter budget

- Training 3.7%
- Patterning 15.9% — $793.77
- Materials 4.6%
- Wet bench 12.3% — $617.48
- Imaging 16.4% — $820.25
- Plasma etching/Oxid… 46.6% — $2,331.67

Mask Reference Table

These mask shapes and dimensions were used for the etches shown in Table 2.

Reference name	Center-to-center spacing [μm]	Width of shape's bounding box [μm]	Shape
R6C3	190	100	
R7C3	190	100	
R2C3	190	100	
R3C4	188.5	100	

R5C3	186.5	100	
R4C3	196.14	100	
R5C1	192.21	100	

# Nuggets

Oxide mask stability

A key component of our fabrication process involves undercutting the oxide mask to form the blade tips before etching the through-holes with the same mask. Thus, it is critical that the mask stays intact despite large undercuts. We found that often the mask was stable but for some designs the mask would flake off and crack during the etching process. This is likely due to stress concentrations introduced in the designs that are unstable during temperature variations during the etch processes. We did not do extensive characterization of what features most likely lead to mask failure, but we would like to give some qualitative insight to future users from our experiments.

> Note: We did not anneal the silicon oxide after chemical vapor deposition. Annealing can improve the integrity of the oxide layer by reducing the magnitude of internal stress as well as prevent internal stress drift over time [6]

General features that lead to mask failure (cracking and flaking off):
- Sharp interior corners. Square openings lead to frequency cracking and failure.
- Long and narrow mask "bridges". Anything >10:1 (length:width) might lead to failure.
- Thin oxide masks. We generally saw more failure with our ~2 micron oxide layer than we did with our 3 micron oxide layer.

Observation 1: Square vs Circular mask opening
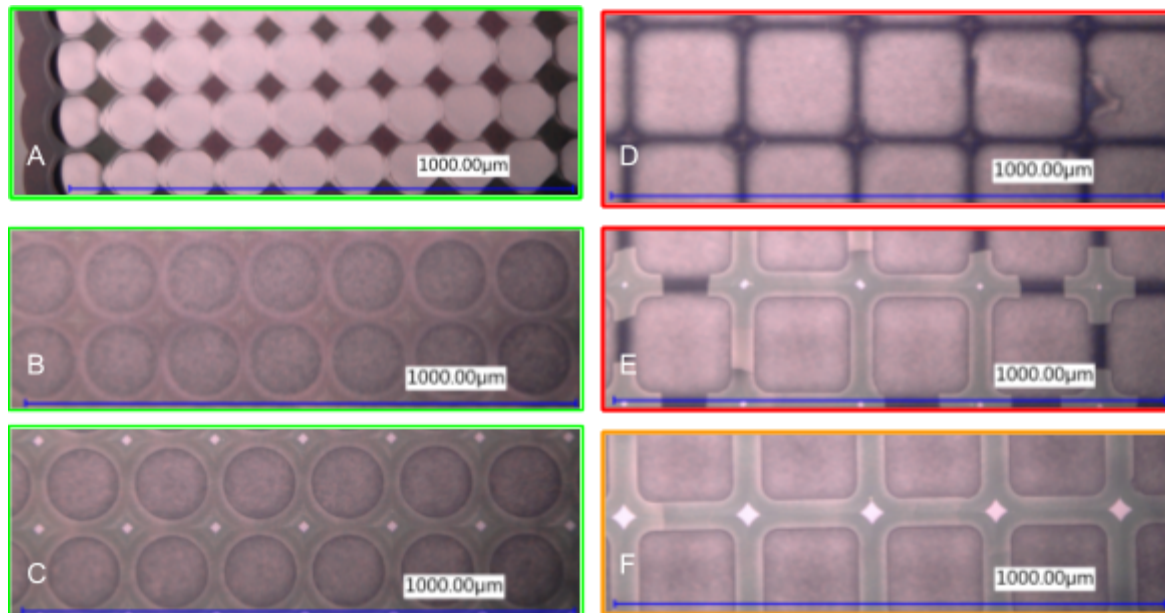
Square oxide mask (D-F) tends to crack/flake once the mask is undercut significantly from etching. This problem did not occur with circular mask openings (A-C) and the mask even remained intact after all supporting substrate was etched (A). This is likely due to stress concentrations in the corners of the square mask.

Observation 2: Aspect ratio dependency.
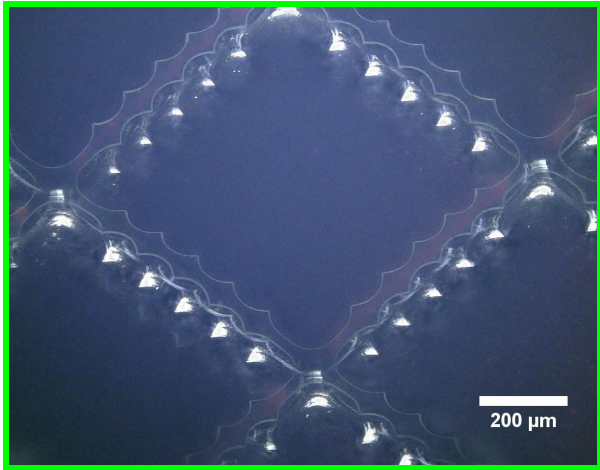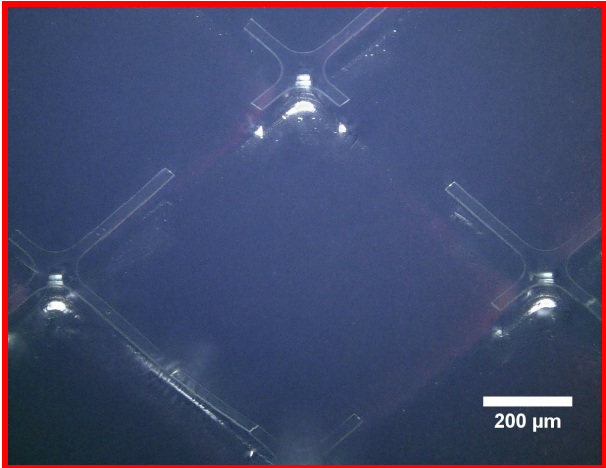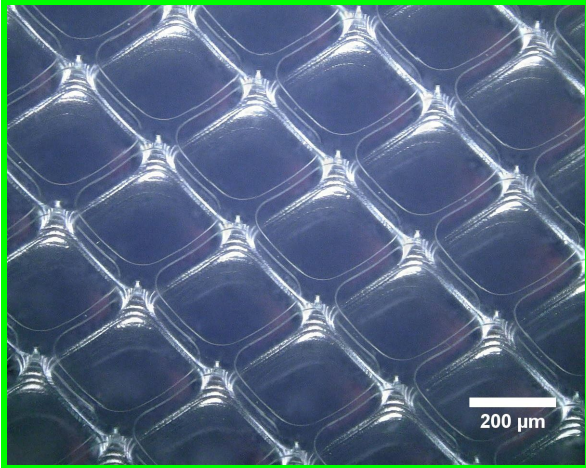
Through-wafer dry etching considerations

Any through-wafer dry etch (DSE_FAT or DSE_Nano) can be limiting and introduce bottom grassing as the etch deepens into the wafer. We noticed that the through-hole at the bottom was significantly smaller in dimension than the mask opening. We addressed the issue of decreasing lateral etch rate with etch depth by increasing the bias voltage of the EtchA step over the course of the through-etch. To address bottom grassing, we appended an isotropic etch step at the end of our through-etch.

Verifying through etch

Using the Keyence digital microscope we were able to verify that we had etched through the silicon wafer down to the silicon oxide hard stop. In the image you can see the junction of a vertical and horizontal line that we were etching. At the junction, you can see the backside oxide showing since we did, in fact, etch through in that location. However, on the areas above, below, to the left, and to the right of center, we did not completely etch through the silicon wafer. By imaging with the keyence directly after etching in the PTDSE we were able to ensure a complete through etch and bring the wafer back into the PTDSE to continue etching.
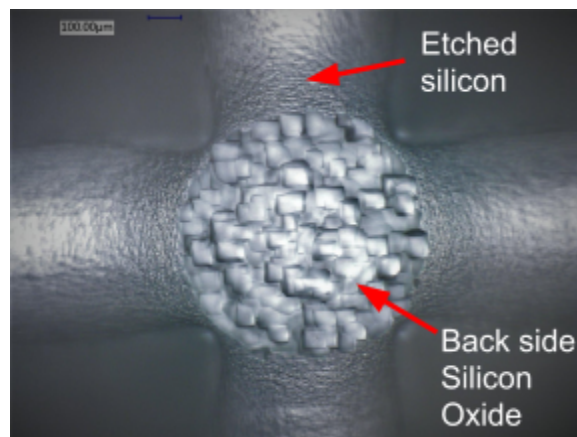

Etch rate dependency on feature size

As expected, feature size influences the resulting etch rate in the PT-DSE. We took some steps to characterize the effect of feature size on horizontal etch rate. We expect a similar feature size dependence on the vertical etch rate. We placed test features around wafers at left, right, top, and bottom locations. While there is expected to be some non-uniformity in the plasma around the wafer, periphery features such as these see mostly similar etch rates. The figure below shows an increase in etch rate for larger mask openings.
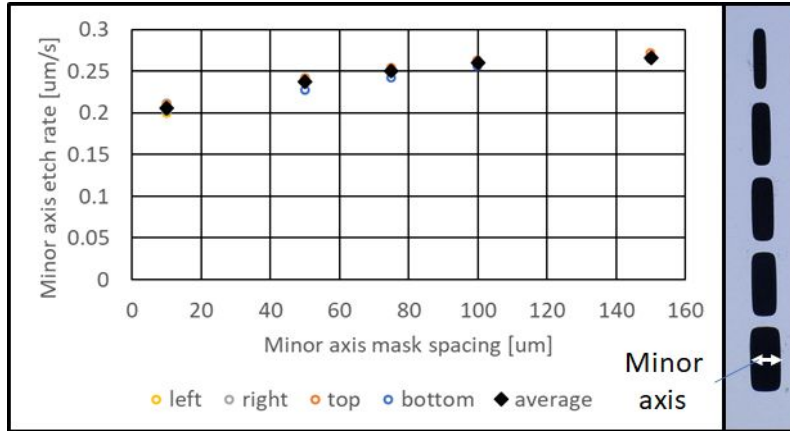
Keyence digital imaging to supplement SEM

We used the Keyence digital microscope to image wafer pieces. This allowed us to determine which samples we wanted to look at on the SEM and look at a larger number of samples relatively quickly. It is cheaper than the SEM and can image a larger number of samples in the same amount of time.
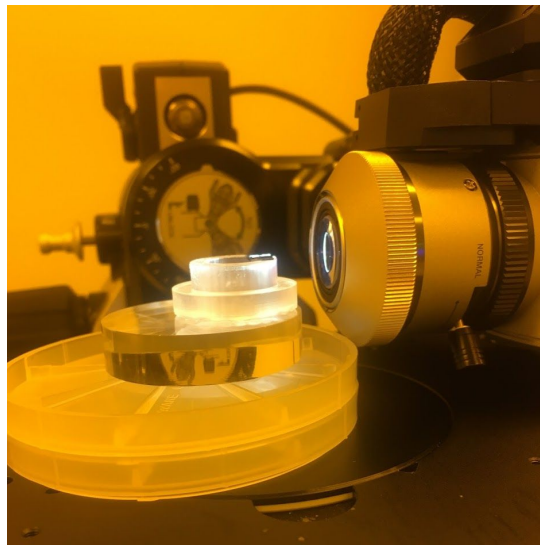
The Keyence digital microscope is rotated 90degrees to take cross-sectional images of cleaved wafer pieces. Acrylic blocks and wafer cases are used to hold the piece in front of the optics. Fine-tuning the height can be done with the stage, being mindful not to collide the stage into the optics.
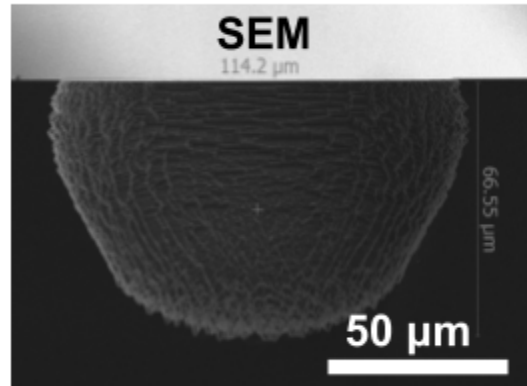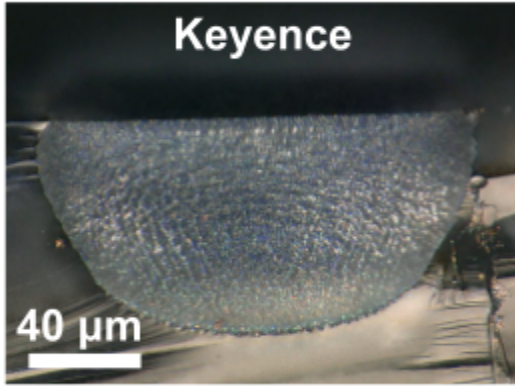
Representative image of a cross-sectional image using the Keyence Digital Microscope (left) and SEM (right) on two different samples.

Bibliography

1. Sun, Y., Campisi, J., Higano, C., Beer, T. M., Porter, P., Coleman, I., True, L., and Nelson, P. S. (2012). Treatment-induced damage to the tumor microenvironment promotes prostate cancer therapy resistance through WNT16B. Nat. Med. *18*, 1359–1368.

2. Li, X., Nadauld, L., Ootani, A., Corney, D. C., Pai, R. K., Gevaert, O., Cantrell, M. A., Rack, P. G., Neal, J. T., Chan, C. W.-M., et al. (2014). Oncogenic transformation of diverse gastrointestinal tissues in primary organoid culture. Nat. Med. *20*, 769–777.

3. Roxhed, N., Griss, P., and Stemme, G. (2007). A method for tapered deep reactive ion etching using a modified Bosch process. J. Micromech. Microeng. *17*, 1087–1092.

4. Stolz, M., Raiteri, R., Daniels, A. U., VanLandingham, M. R., Baschong, W., and Aebi, U. (2004). Dynamic elastic modulus of porcine articular cartilage determined at two different levels of tissue organization by indentation-type atomic force microscopy. Biophys. J. *86*, 3269–3283.

5. Singh, A., Brito, I., and Lammerding, J. (2018). Beyond tissue stiffness and bioadhesivity: advanced biomaterials to model tumor microenvironments and drug resistance. Trends Cancer *4*, 281–291.

6. Fu, J., Shang, H., Li, Z., Wang, W., and Chen, D. (2017). Thermal annealing effects on the stress stability in silicon dioxide films grown by plasma-enhanced chemical vapor deposition. Microsyst. Technol. *23*, 2753–2757.